Typhoon-induced phytoplankton blooms and primary productivity increase in the western North Pacific subtropical ocean

I.-I. Lin[1]

Received 30 September 2011; revised 25 November 2011; accepted 28 November 2011; published 28 March 2012.

[1] Using multiple satellite observations and series of numerical experiments, this work systematically studied phytoplankton blooms induced by tropical cyclones in the western North Pacific subtropical ocean (WNPSO) because WNPSO is among the world oceans where most number of intense tropical cyclones are found. All eleven typhoon cases passing the study domain in 2003 were examined in detail. It was observed that only two typhoons (18%) were able to induce phytoplankton blooms (chlorophyll-a concentration increased from ≦0.1 mg m^{-3} to 0.4–0.8 mg m^{-3}) and strong sea surface temperature cooling of −2.5 to −6°C. The other nine typhoons, including the most intense tropical cyclone on Earth in 2003 (i.e., supertyphoon Maemi), were not able to induce phytoplankton blooms and the associated sea surface temperature cooling was weak (0 to −1.5°C). Using series of numerical experiments, it was found that the presence of warm ocean eddy can effectively isolate the cold, nutrient-rich water to be entrained to the surface ocean. Under this situation, even category 5 typhoon Maemi at its peak intensity of 150 kts could not induce phytoplankton bloom in the WNPSO. The weak responses of the other eight typhoons were due to insufficient wind intensity and transit time (caused by relatively small storm size and fast translation speed) in this deep nutricline/mixed layer ocean. As a result, the total annual primary production increase induced by typhoons in the WNPSO was estimated to be $\sim 3.27 \times 10^{12}$ g C (0.00327 Pg), equivalent to 0.15% of the global annual anthropogenic CO_2 uptake. This suggests that though WNPSO has the highest number and intensity of tropical cyclones among the world oceans, tropical cyclones in the WNPSO have little contribution to enhance biological carbon fixation in the context of global carbon-climate system.

Citation: Lin, I.-I. (2012), Typhoon-induced phytoplankton blooms and primary productivity increase in the western North Pacific subtropical ocean, *J. Geophys. Res.*, *117*, C03039, doi:10.1029/2011JC007626.

1. Introduction

[2] The western North Pacific subtropical ocean (WNPSO) is among the world's oceans where tropical cyclones (typhoons), both highest in number and intensity, are found [*Lin et al.*, 2009a; *D'Asaro et al.*, 2011]. Since the intense wind of typhoons can induce strong ocean mixing and upwelling [*Price*, 1981; *Dickey et al.*, 1998; *Lin et al.*, 2003a; *Sanford et al.*, 2011], deeper-ocean nutrients could be brought to the nutrient-depleted upper ocean to induce ocean biogeochemical response and increase in primary productivity [*Lin et al.*, 2003b; *Babin et al.*, 2004; *Zheng and Tang*, 2007; *Shang et al.*, 2008]. Existing studies in the WNPSO and neighboring seas primarily focus on individual cases where evident blooms were observed [*Lin et al.*, 2003b; *Zheng and Tang*, 2007; *Chang et al.*, 2008; *Shang et al.*, 2008]. However, the many other no-bloom cases were neglected. It is thus desirable to conduct an objective study to examine all cases without bias and to explore the overall annual contribution to primary productivity of all typhoons in the WNPSO in the context of global carbon-climate system [*Falkowski et al.*, 2000; *Sabine et al.*, 2004; *Lin et al.*, 2011a].

[3] In this research, we employed four types of satellite remote sensing data and three models to conduct our investigation. The satellite data includes (1) chlorophyll-a (Chl-a) concentration from the NASA/Sea-viewing Wide Field-of-View (SeaWiFS) and the Moderate Resolution Imaging Spectroradiometer (MODIS) sensors [*O'Reilly et al.*, 1998; *Carder et al.*, 1999], (2) sea surface temperature (SST) from the Tropical Rainfall Measuring Mission (TRMM) Microwave Imager (TMI) and the Advanced Microwave Scanning Radiometer (AMSR-E) [*Wentz et al.*, 2000], (3) ocean surface wind vectors from the QuikSCAT and the SeaWinds sensors [*Liu et al.*, 1998], and (4) sea surface height anomaly (SSHA) data from the TOPEX/Poseidon and JASON-1 altimeters [*Fu et al.*, 1994; *Fu and Cazenave*, 2001]. The three models used were (1) the Vertically Integrated Primary Production (VGPM) model from *Behrenfeld and Falkowski*

[1]Department of Atmospheric Sciences, National Taiwan University, Taipei, Taiwan.

0148-0227/12/2011JC007626

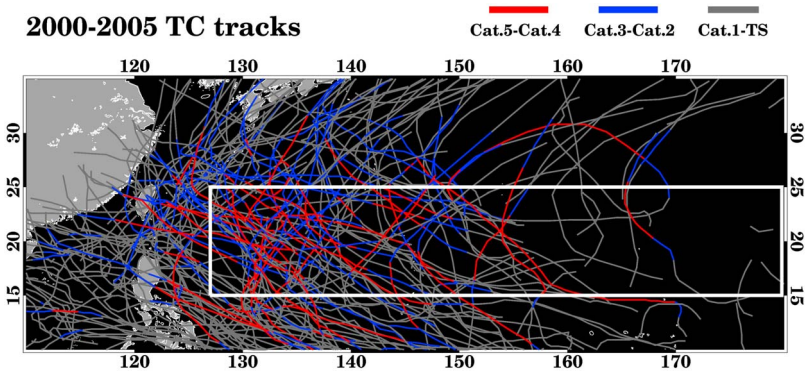

Figure 1. Tracks of typhoons observed between 2000 and 2005 with the study area depicted in the box. Typhoon track segments are depicted in color according to intensity (tropical storm–category 1, gray; category 2–3, blue; category 4–5, red). Data source: best track typhoon data from the U.S. JTWC.

[1997], (2) 1-D ocean mixed layer model based on the work of *Mellor and Yamada* [1982], and (3) 3-D ocean mixed layer model based on the work by *Price et al.* [1994]. All typhoons in the year of 2003 passing over the WNPSO were studied. There were two reasons to choose 2003. First, it is a year in which most numbers of relevant satellite sensors were operational in orbit (e.g., QuikSCAT and SeaWinds), thus can maximize observations. Second, as WNPSO can experience large interannual variability due to El Niño/La Niña events [*McPhaden*, 1999; *Kug et al.*, 2009; *Kim et al.*, 2010], a normal year is chosen to assess the contribution.

2. Data and Method

[4] The study region, WNPSO, is defined as between 15 and 25°N, 127 and 180°E, corresponding to the region where most number of intense typhoons are found (Figure 1). In 2003, there were 11 typhoon cases passing over the domain. The typhoon track, intensity, and size data are based on the best track data of the U.S. Joint Typhoon Warning Centre (JTWC) (Table 1).

[5] Daily Chl-a observations from level 3, 9 km spatial-resolution SeaWiFS and 4 km resolution MODIS data were examined to identify changes in biogeochemical response due to typhoons' passing. Corresponding SST data from TRMM and AMSR-E [*Wentz et al.*, 2000] was used to observe the associated typhoon-induced SST cooling [*Price*, 1981; *Dickey et al.*, 1998; *Lin et al.*, 2003b; *Shang et al.*, 2008]. Wind vectors from QuikSCAT and SeaWinds [*Liu et al.*, 1998] were for typhoon structure. SSHA data from the TOPEX/Poseidon and Jason-1 altimeters [*Fu et al.*, 1994; *Fu and Cazenave*, 2001] were used to observe ocean precondition (e.g., presence of mesoscale eddies) before typhoons' passing, as well as identifying posttyphoon ocean condition [*Shay et al.*, 2000; *Lin et al.*, 2005, 2008, 2009b, 2010, 2011b; *Pun et al.*, 2007, 2011; *Goni et al.*, 2009; *Ali et al.*, 2012]. Among these satellite data, the SST, surface wind vector, and SSHA were derived from microwave signals. Thus it had the advantage of cloud penetration capability and observations will not be hindered due to presence of cloud cover [*Fu et al.*, 1994; *Liu et al.*, 1998; *Wentz et al.*, 2000]. The spatial resolutions of the SST and wind vector were both 25 km. The along-track resolution of the altimetry SSHA was 5.5 km and the swath gap was 150 km [*Fu et al.*, 1994].

[6] To assess the impact to primary productivity, the Vertically Generalized Production Model from *Behrenfeld and Falkowski* [1997] was used to estimate the increase in primary production due to typhoon-induced phytoplankton

Table 1. Summary of the 11 Typhoon Cases in 2003, Arranged in Descending Order of Peak Intensity (Based on 1 min Maximum Sustained Wind Speed From the Best Track Data of JTWC) When Passing Over the Study Domain[a]

Typhoon Case	Date/Time of the Observed Maximum Intensity in the Study Domain	Intensity in kts[b]	Translation Speed Uh (m s^{-1})	Size in Diameter of 64 kts Wind (km)	Transit Time (h)	Initial D26 (m)	ΔSST[c] (°C)	ΔChl-a[c] (mg/m^3)
Maemi	0910/00Z	150 (C5)	3.4	188	15	114	−0.34	0.01
Lupit	1127/12Z	145 (C5)	3.6	257	20	95	−2.88	0.09
Ketsana	1021/12Z-1022/12Z	125 (C4)	1.7	210	34	93	−3.14	0.06
Chan-Hom	0523/18Z-0525/00Z	115 (C4)	6	139	6	44	−0.17	0.02
Parma	1029/12Z	115 (C4)	5.7	164	8	39	−1.22	0
Etau	0806/00Z-0806/12Z	95 (C2)	6.5	109	5	61	−1.87	−0.02
Dujuan	0831/12Z	95 (C2)	7.9	189	7	95	0.02	−0.01
Krovanh	0821/06Z-0821/12Z	65 (C1)	5.7	97	5	70	−0.19	−0.01
Koppu	0927/06Z-0928/00Z	60 (TS)	5.3	125	7	48	−1.08	0.01
Choi-Wan	0919/00Z	55 (TS)	6.2	83	4	89	−0.3	0.01
Yan-Yan	0119/12Z-0120/00Z	40 (TS)	6	58	3	129	−0.27	0.01

[a]The time is the UTC time (denoted as Z). The intensity category is according to the Saffir-Simpson tropical cyclone scale where tropical storm (TS), 34–63 kts; category 1, 64–82 kts; category 2, 83–95 kts; category 3, 96–112 kts; category 4, 113–135 kts; category 5, >135 kts. The seventh column summarizes the initial subsurface D26 based on in situ profiles. The eighth and ninth columns summarize the along-track-averaged SST and Chl-a responses based on Figure 3.
[b]Category in Saffir-Simpson scale.
[c]After minus before.

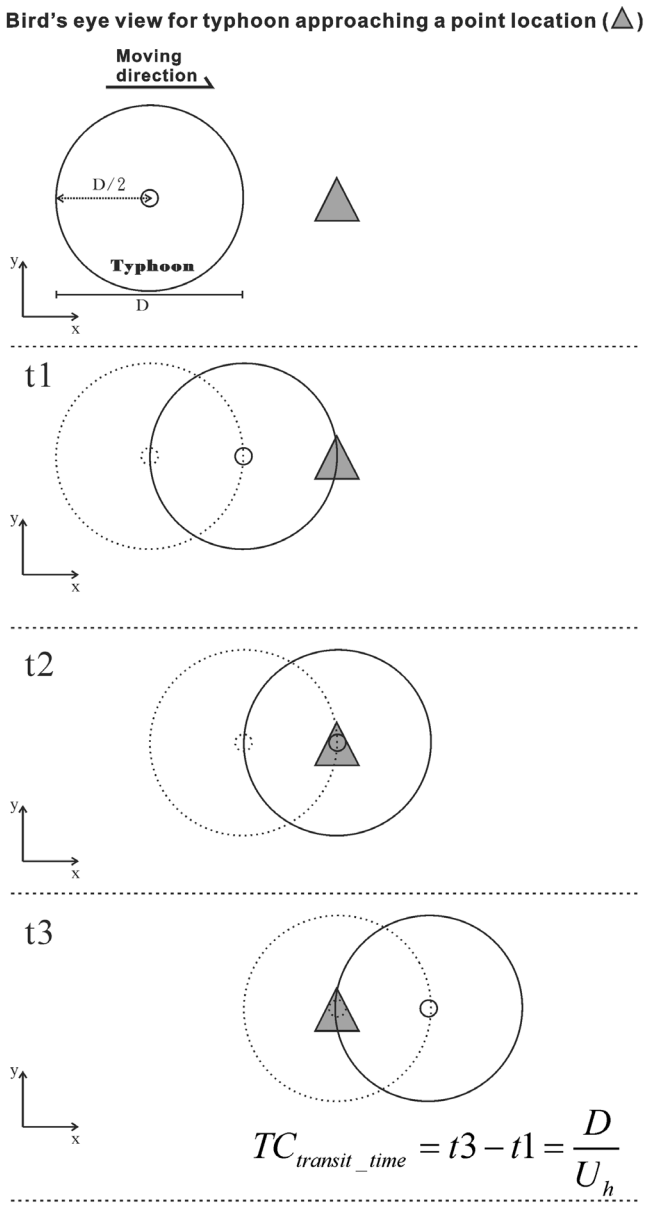

Figure 2. Schematic diagram showing the 1-D MY mixed layer model simulation of a typhoon approaching a point location in the ocean. The transit time is calculated as D/U_h, where D is the typhoon's vortex size in diameter and U_h is translation speed [after *Lin et al.*, 2008].

bloom events. With input from the observed satellite Chl-a concentration and SST (for estimation of the photoadaptive variables), the integrated primary productivity (IPP) and total carbon fixation (integration of IPP over bloom area and bloom period) were calculated [*Behrenfeld and Falkowski*, 1997; *Lin et al.*, 2003b].

[7] After observations, series of ocean numerical experiments were conducted to explore the mechanistic link between typhoon parameters (i.e., intensity in wind speed, translation speed, and size) and ocean's responses in SST reduction [*Price*, 1981; *Dickey et al.*, 1998; *Lin et al.*, 2003a; *Sanford et al.*, 2011]. The Mellor-Yamada (MY) 1-D ocean mixed layer model was run [*Mellor and Yamada*, 1982; *Jacob et al.*, 2000] with wind forcing from JTWC's best track 10 min maximum sustained wind. The drag coefficient (C_d) was the high wind coefficient from *Powell et al.* [2003]. Initial inputs were the in situ ocean depth-temperature profiles searched from the Argo floats [*Gould et al.*, 2004] and the U.S. National Oceanic and Atmospheric Administration (NOAA)'s Global Temperature and Salinity Profile Program (GTSPP) [*Keeley et al.*, 2003] databases. Profiles were searched along typhoons' tracks to within 1° radius and within 1 week prior to typhoons' passing. For cases where no in situ profiles could be found, climatological depth-temperature profiles from the NOAA/World Ocean Atlas 2001 [*Stephens et al.*, 2002] were used.

[8] The 1-D MY model was run according to the time of typhoon's passing, i.e., Tropical Cyclone (TC)'s transit time ($TC_{transmit-time}$) [*Cione and Uhlhorn*, 2003; *Lin et al.*, 2008, 2009]. As explained in detail by *Lin et al.* [2008] and depicted in Figure 2, due to differences in typhoon's size and translation speed, the time needed for a typhoon to pass over a specific point location in ocean is different from case to case [*Cione and Uhlhorn*, 2003]. As in the work by *Cione and Uhlhorn* [2003] and *Lin et al.* [2008], $TC_{transmit-time}$ can be calculated as

$$TC_{transit-time} = D/U_{h,} \quad (1)$$

where D is typhoon's vortex diameter (here the 64 kts radius is used) and U_h is translation speed.

[9] For typhoon cases with slower translation speeds (typically $U_h \leqq 4$ ms^{-1}), the 3-D ocean mixed layer model [*Price et al.*, 1994] was run in addition to the 1-D MY model. This is because 1-D ocean mixed layer models only consider the contribution of entrainment mixing. However, under slow translation speeds, it is also necessary to consider the contribution from upwelling in addition to entrainment mixing [*Price*, 1981; *Lin et al.*, 2003b]. Therefore for typhoon cases of $U_h \leqq 4$ ms^{-1}, additional numerical experiments using the 3-D model were conducted to include the contribution from upwelling.

3. Observations of Pretyphoon Conditions and Posttyphoon Ocean Responses

[10] According to peak intensity when passing over WNPSO, the eleven typhoon cases were ranked (Table 1). Supertyphoon Maemi [*Lin et al.*, 2005] was the most intense, followed by supertyphoon Lupit. As in Table 1, both Maemi and Lupit belong to the highest-intensity category of 5 in the Saffir-Simpson tropical cyclone scale. As their peak intensity exceeded 130 kts, they are also called supertyphoons. The third intense typhoon was Ketsana. It was an upper category 4 typhoon of peak at 125 kts, only 5 kts below the supertyphoon criterion of 130 kts. Following Ketsana were two other lower category 4 typhoons, Chan-Hom and Parma. Their peak intensity was both 115 kts. There was no category 3 typhoon found to pass the WNPSO in 2003. As for category 2, there were two cases (Dujuan and Etau), for category 1 one case (Krovanh), and lastly, 3 cases (Koppu, Choi-Wan, Yan-Yan) for tropical storms (Table 1).

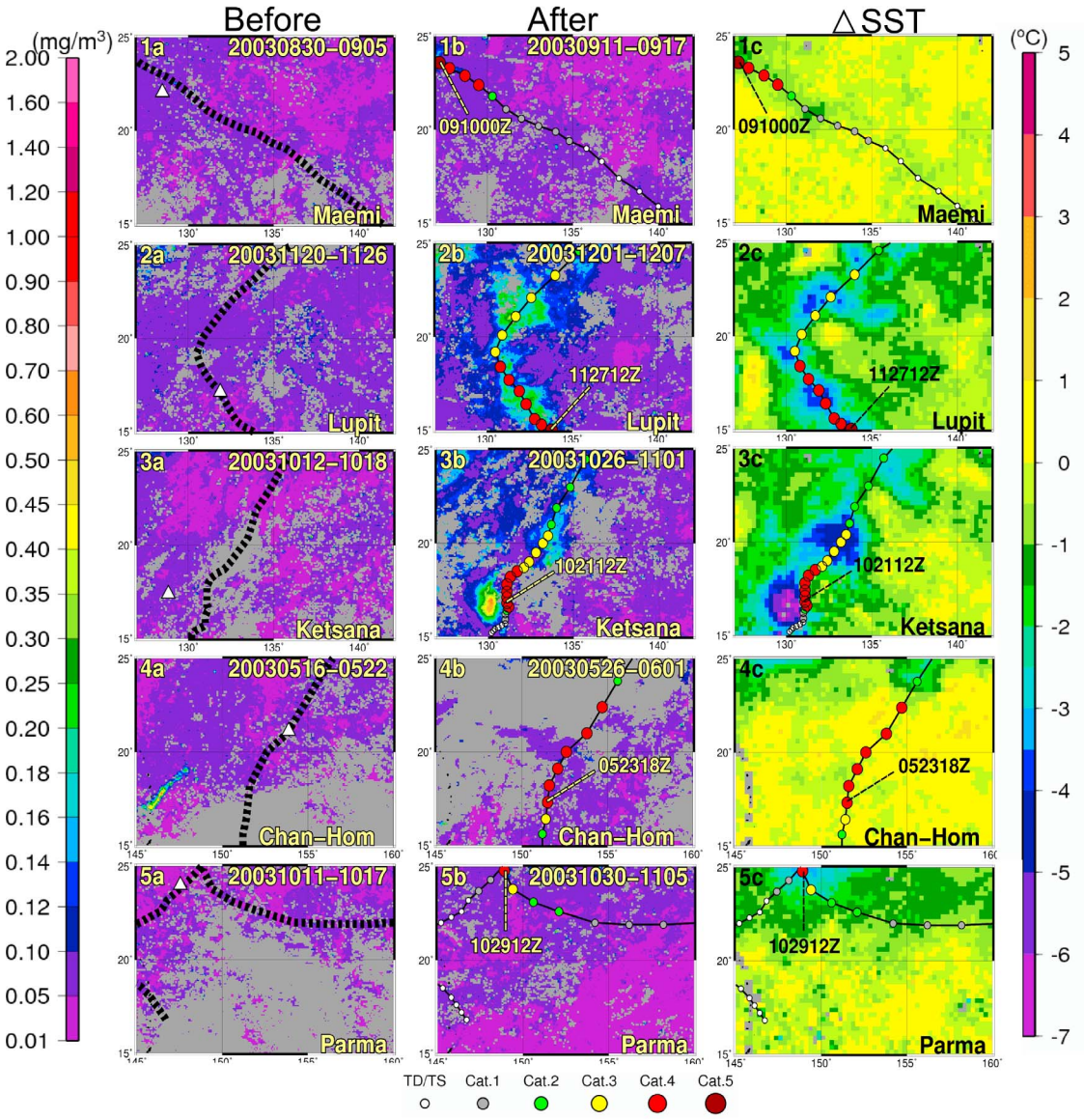

Figure 3. Observations of weekly averaged Chl-a concentration (left) before and (middle) after the passing of the 11 typhoon cases (tracks overlaid). (right) The corresponding SST difference (posttyphoon SST subtracted by before-typhoon SST) is depicted. Locations of the depth-temperature profiles are depicted by triangles. The observed typhoon intensity in Saffir-Simpson scale is depicted by color bullets.

[11] Figure 3 illustrates observations of weekly averaged Chl-a concentration before (Figure 3, left) and after (Figure 3, middle) the passing of the eleven typhoons. In Figure 3 (right), the corresponding SST difference (posttyphoon SST subtracted by before-typhoon SST) is depicted. The eleven rows in Figure 3 are ordered according to the peak intensity ranking as in Table 1. Observing Figure 3 (left and middle), it can first be noted that besides Lupit (Figure 3, panel 2b) and Ketsana (Figure 3, panel 3b), no evident biogeochemical responses could be found after the passing of typhoons. Before typhoons' passing, Chl-a concentration was predominantly $\leqq$0.1 mgm^{-3} for all eleven cases (Figure 3, left). After the passing of typhoons, Chl-a concentration increased to $\sim$0.3–0.4 mgm^{-3} for Lupit case (Figure 3, panel 2b) and to $\sim$0.3–0.8 mgm^{-3} for Ketsana case (Figure 3, panel 3b). However, the posttyphoon Chl-a concentration for all the other cases showed Chl-a concentration of $\leqq$0.1 mgm^{-3}, similar to the pretyphoon values.

[12] The corresponding SST cooling maps (Figure 3, right) show consistency with the Chl-a observations. It can be observed that the cooling response induced by Lupit was ~ -2.5 to -3.5°C (Figure 3, panel 2c) and ~ -2.5 to -6.5°C by Ketsana (Figure 3, panel 3c). However, the SST cooling of all the other cases were mostly around 0 to -1.5°C (Figure 3, right). In addition, since SST observations are from cloud-penetrating microwave sensors, it support the results of the SeaWiFS optical observations that indeed the responses of Lupit and Ketsana were the strongest while the responses of the other nine cases were much weaker.

[13] Why only Lupit and Ketsana could induce significant biogeochemical and SST cooling responses in the WNPSO?

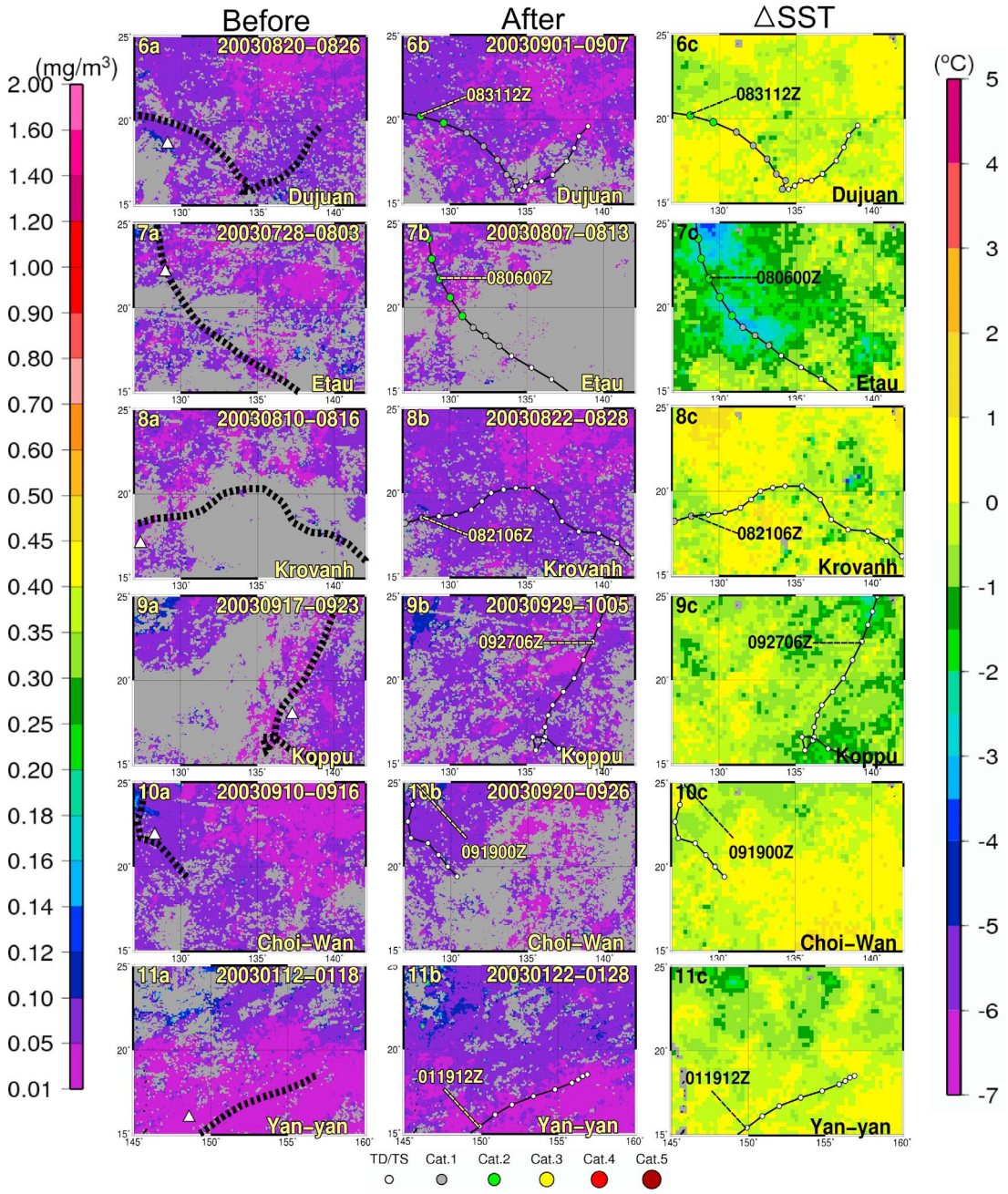

Figure 3. (continued)

Why all the other cases, including Maemi [*Lin et al.*, 2005], the most intense tropical cyclone on Earth in 2003, could not induce such strong responses? In addition, when comparing the responses of Lupit and Ketsana, it can be seen that both SST cooling and Chl-a responses induced by Lupit (Figure 3, panels 2b and 2c) were weaker than Ketsana (Figure 3, panels 3b and 3c). However, Ketsana's intensity (category 4) was weaker than Lupit's (category 5) (Table 1).

[14] Examine the along-track SST and Chl-a responses with respect to the observed typhoon parameters, it was found that in general, the stronger responses from Ketsana and Lupit were associated with higher typhoon intensity (≧125 kts, Figures 4a and 4d) and longer transit time (≧20 h, Figures 4b and 4e). As for the case of Maemi, though it had the highest intensity of 150 kts (star in Figures 4a and 4d), its transit time was shorter (15 h, see star in Figures 4b and 4e) than the cases of Ketsana and Lupit. In addition, Maemi was associated with deeper initial subsurface depth of the 26°C isotherm (D26) of ∼114 m, suggesting cold water located in deeper subsurface and more difficult to entrain the

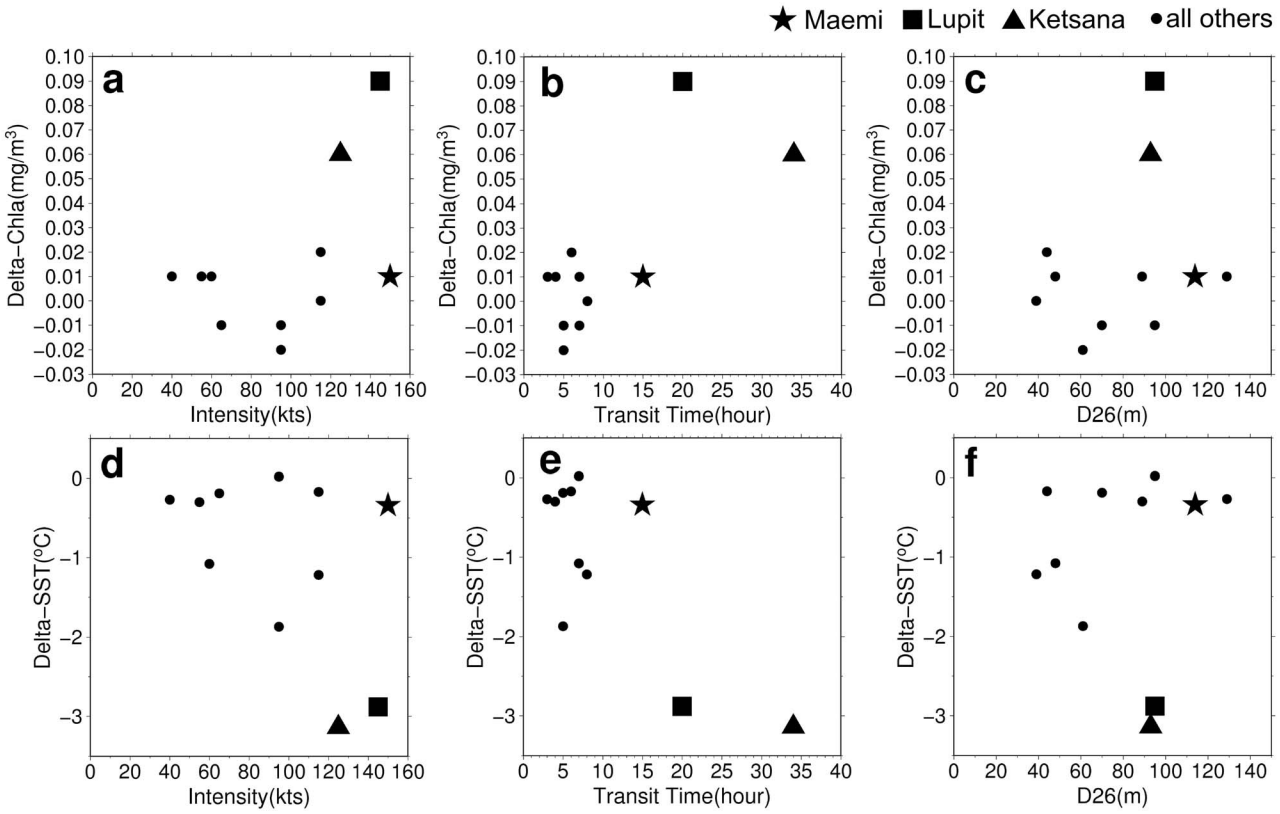

Figure 4. Based on Table 1, the observed along-track SST and Chl-a responses with respect to the observed typhoon parameters. Chl-a responses versus (a) intensity, (b) transit time, and (c) initial D26. SST responses versus (d) intensity, (e) transit time, and (f) initial D26.

cooling response. Using series of numerical experiments, these issues were further investigated quantitatively.

4. Numerical Experiments

[15] Figure 5 depicts the results of the 1-D typhoon-induced SST cooling simulation with respect to transit time. Consistency can be found as in the observation that Ketsana's response was the strongest (dark blue bullet in Figure 5), followed by Lupit (green bullet), while the responses of the other cases were weaker. It can be seen that give its 34 h transit time, the simulated SST cooling induced by Ketsana was ∼−3.1°C, ∼−2.5°C for Lupit at its 20 h transit time, and ∼0 to −1.6°C for the other cases (see colored bullets in Figure 5). In the following, simulation results of each case are discussed in detail according to the order given in Table 1. Also, since Lupit represented the baseline case which was able to induce phytoplankton bloom in the WNPSO, it was used as a reference in diagnose.

4.1. Supertyphoon Maemi (Peak Intensity: Category 5, 150 kts)

[16] Figure 6a depicts the simulation results of SST reduction using the 1-D MY model for the Maemi case (red curve). The simulated SST reduction of Lupit case (green curve) is also plotted as a reference. It can be seen that though Maemi's wind speed was more intense (150 kts) than Lupit's (145 kts), the SST cooling induced by Maemi was

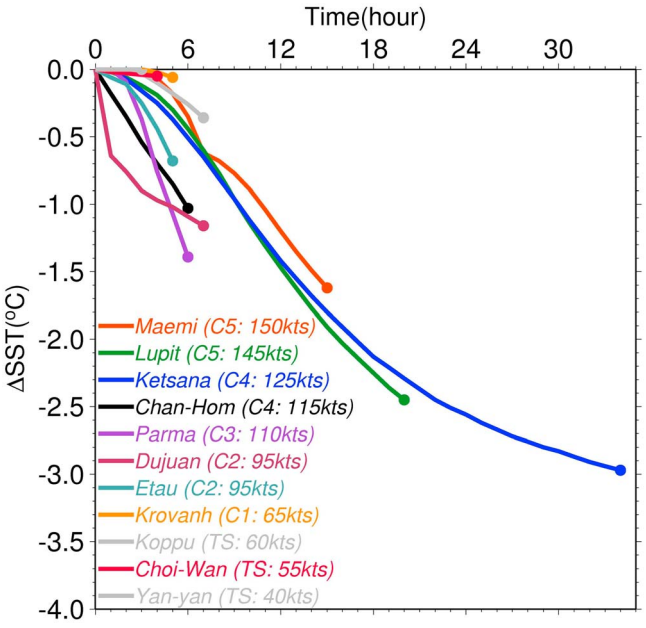

Figure 5. Results from the 1-D ocean mixed layer numerical experiments for the 11 cases. The *y* axis depicts typhoon-induced SST cooling response. The *x* axis depicts typhoon's transit time. Color bullets denote the SST cooling at the end of the transit time for each case.

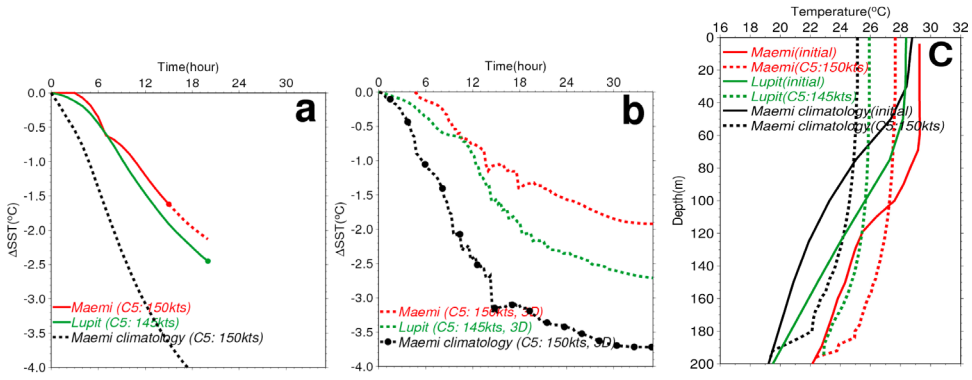

Figure 6. (a) Comparison of SST cooling response for Maemi case, Lupit case, and Maemi climatological case (i.e., no-eddy run) using the 1-D MY model [*Mellor and Yamada*, 1982]. The *x* axis depicts transit time. Color bullets denote the SST cooling at the end of the transit time. (b) As in Figure 6a but for simulation results using the 3-D ocean mixed layer model by *Price et al.* [1994]. (c) Comparison of the pretyphoon (solid profiles) and after-typhoon (at the end of transit time, dashed profiles) depth-temperature profiles for the three simulations.

weaker than in the Lupit case. Observing the initial profiles, one can see that there was a difference in the initial ocean preconditions. For the Maemi case, the pretyphoon upper ocean thermal structure (red solid profile in Figure 6c) was warmer than in the case of Lupit (green solid profile in Figure 6c). It can be seen that Maemi passed by a region not only with warm SST of 29.2°C, the mixed layer was also deep, reaching 80 m while the depth of the 26°C isotherm (D26) reaching 120 m. Why such deep, warm structure? Based on the TOPEX/Poseidon and JASON-1 SSHA observations, it could be found that this was due to the presence of two preexisting prominent warm ocean eddies, as characterized by positive SSHA of 20 to 40 m (Figure 7a). It can be observed in Figure 7b that even after the passing of supertyphoon Maemi, the warm ocean eddies were still robust, as characterized by positive SSHA. In contrast, for the Lupit and Ketsana cases, the posttyphoon SSHA was characterized by evident negative SSHA of −20 to −40 cm along the track (Figures 7d and 7f). Similar comparison in SST observation is seen that before and after Maemi's passing, SST dropped slightly from ∼29°C to ∼28°C (Figures 8a and 8b). However, for the Lupit case, SST dropped from ∼27–28.5°C to ∼24–25°C (Figures 8e and 8f), for the Ketsana case, from ∼28.5–30°C to ∼23–24°C (Figures 8c and 8d).

[17] If without the presence of warm eddy, the mixed layer and the subsurface D26 would be much shallower (e.g., mixed layer ∼30 m and D26 ∼ 70 m), as depicted in the climatological profile of the same location (black solid profile in Figure 6c) [*Stephens et al.*, 2002]. In other words, without warm eddies, the cold, nutrient rich water would be much closer to the surface than under the warm eddy condition. Using the climatological profile as an initial profile and forced by the Maemi wind, additional numerical simulation was performed to simulate the "no-eddy" condition. From Figure 6a, one can see that under the no-eddy condition, the SST cooling could reach as much as −4°C at transit

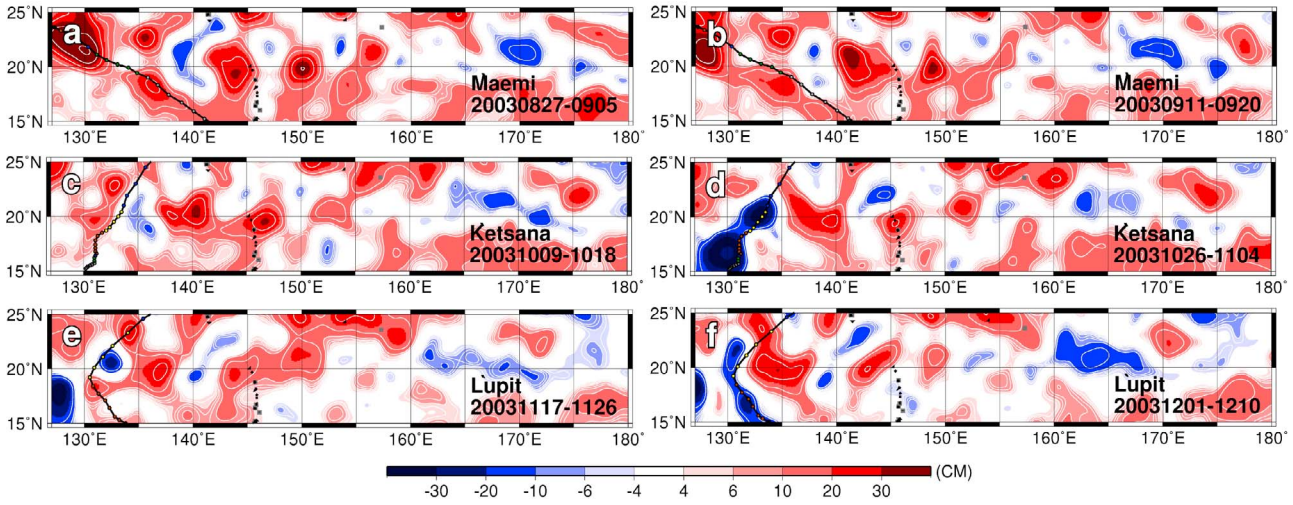

Figure 7. The (a) before-typhoon and (b) posttyphoon SSHA observation for the Maemi case, (c and d) for the Ketsana case, and (e and f) for the Lupit case.

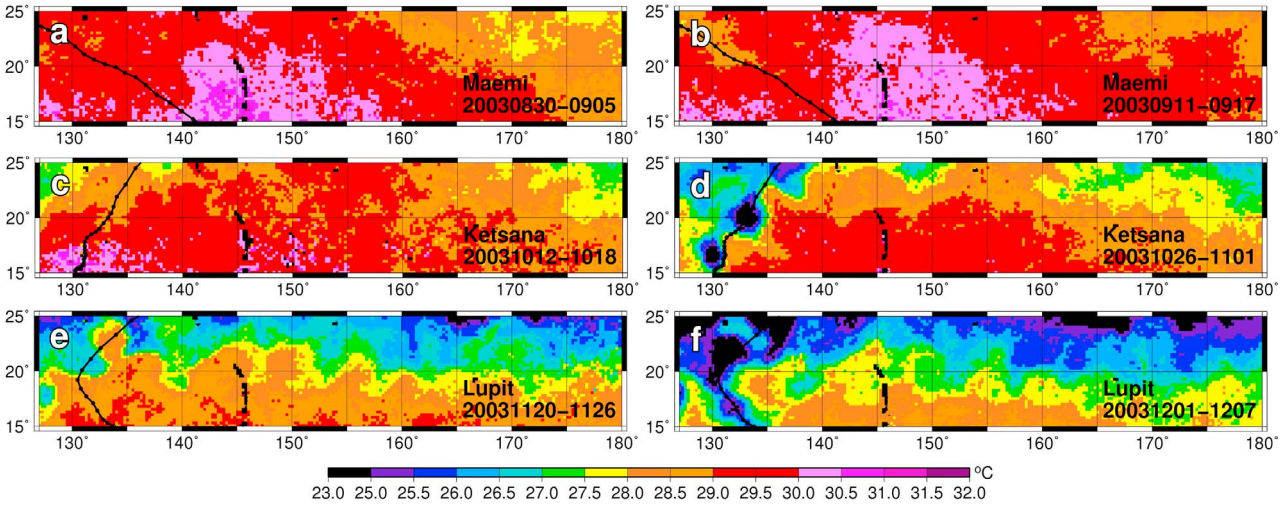

Figure 8. (a–f) As in Figure 7 but for the pretyphoon and posttyphoon SST observation.

time of 15 h (black dotted curve), even stronger cooling response than in the cases of Lupit.

[18] Besides from the presence of warm eddies, the transit time of Maemi (15 h) was also shorter than Lupit's transit time of 20 h (Table 1). Thus there was also more time for Lupit to induce stronger responses than Maemi (see green and red bullets in Figure 6a). However, the main factor for Maemi's weaker response than Lupit was still the preexisting warm ocean eddy and not the transit time. This can be seen by additional numerical simulation to prolong Maemi's transit time (see dotted part of the red curve in Figure 6a) that even at 20 h transit time, Maemi's cooling response was still weaker than Lupit's. Finally, because the translation speeds of Maemi and Lupit were both $\leqq 4$ ms^{-1} (Table 1), an additional set of simulations using the 3-D ocean mixed layer model was conducted [*Price et al.*, 1994]. As depicted in Figure 6b, the results were very similar to the results using the 1-D MY model, also showing the weaker cooling response of Maemi due to the presence of warm ocean eddy.

4.2. Supertyphoon Lupit (Peak Intensity: Category 5, 145 kts) and Intense Typhoon Ketsana (Peak Intensity: Category 4, 125 kts)

[19] From Figure 3, it can be observed that though both Ketsana and Lupit could induce blooms in the WNPSO, the response induced by category 4 typhoon Ketsana (peak intensity: 125 kts, Figure 3, panels 3b and 3c) was stronger than the response induced by category 5 typhoon Lupit (peak intensity: 145 kts, Figures 3, panels 2b and 2c). Figure 9a depicts the simulation results of these two cases using the 1-D MY model. From Figure 9a, it can be observed that the cooling responses for these two cases were quite similar from 0 to 20 h. However, as Ketsana's transit time was 34 h, much longer than the 20 h transit time of Lupit (green bullet in Figure 9a), there was longer time for ocean to be under the forcing of Ketsana to induce stronger response (red bullet in Figure 9a). If given Lupit longer response time to 34 h (green dotted curve in Figure 9a), it was possible for Lupit to induce similar response as Ketsana.

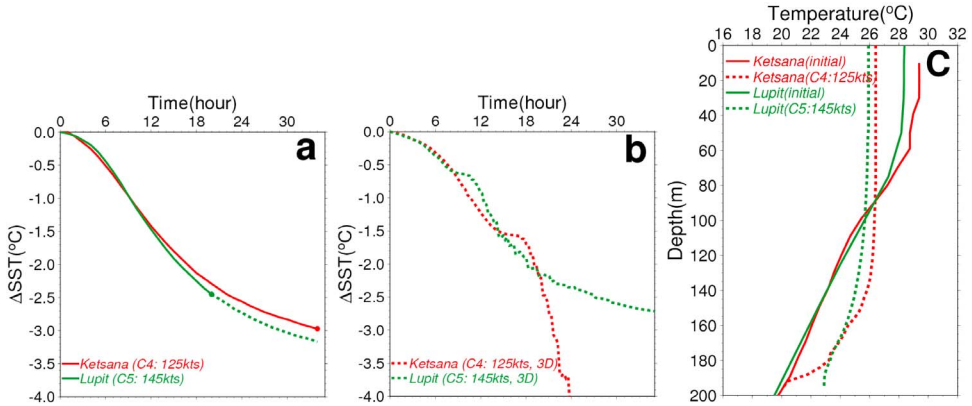

Figure 9. (a) Comparison of SST cooling response for Ketsana and Lupit cases using the 1-D MY model. The *x* axis depicts transit time. Color bullets denote the SST cooling at the end of the transit time for each case. (b) As in Figure 9a but for simulation results using the 3-D ocean mixed layer model. (c) Comparison of the pretyphoon (solid profiles) and after-typhoon (at the end of transit time, dashed profiles) depth-temperature profiles for the two simulations.

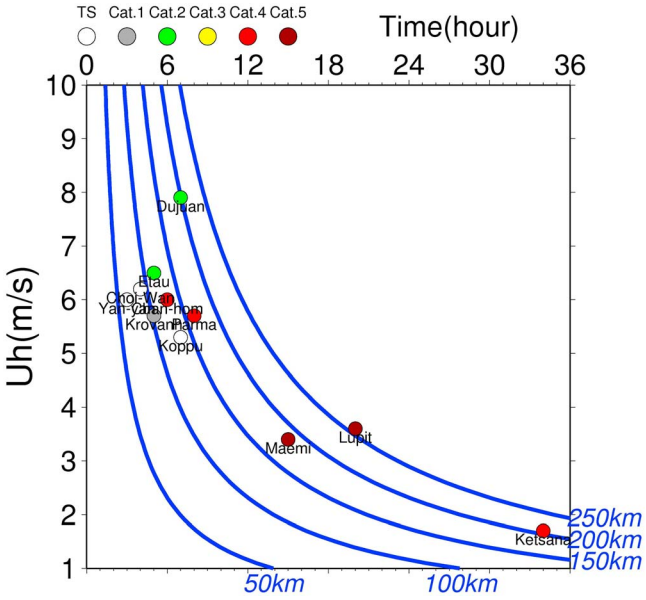

Figure 10. Based on equation (1), the relationship between transit time (upper x axis), vortex size D (in 64 kts diameter), and translation speed U_h (y axis) is depicted. The transit time of the 11 cases are depicted by color bullets.

[20] From equation (1), one can see that transit time is a function of vortex diameter D and translation speed, U_h. This function is plotted in Figure 10 as a reference. It can be seen that the larger the diameter, the slower the translation speed, the longer the transit time. It can be found in Table 1 that the reason why Ketsana had longer transit time than Lupit was mainly due to its slower translation speed and not the size because the vortex diameter of Ketsana was smaller than Lupit's (Table 1). From Figure 10 and Table 1, it can be seen that due to Ketsana's slow translation speed of $U_h \sim 1.7$ ms^{-1}, it had a much longer transit time than Lupit because Lupit's U_h was $\sim$3.6 ms^{-1}. Further, the slower the translation speed, the stronger the ocean's cooling response because in addition to entrainment mixing, upwelling can be induced [*Price*, 1981]. This can be supported by additional numerical simulation using the 3-D model that the SST cooling of Ketsana (dotted red curve) was much stronger than in the case of Lupit (dotted green curve) (Figure 9b).

4.3. Category 4 Typhoon Chan-Hom (Peak Intensity: 115 kts) and Parma (Peak Intensity: 115 kts)

[21] From Figure 3, one finds that the responses by the other two category 4 typhoons, i.e., Chan-Hom (Figure 3, panels 4b and 4c) and Parma (Figure 3, panels 5b and 5c), were weaker than Lupit's responses too. Numerical simulations reflected this situation. Figure 11a depicts the results of Chan-Hom (red curve). It can be found that though Chan-Hom's cooling response (red curve) was stronger than Lupit's (green curve) from 0 to 6 h, due to its very short transit time of 6 h, the cooling response was only ~ -1.1°C (see red bullet in Figure 11a). From Table 1 and Figure 10, it can be seen that the reason for such short transit time was due to both the smaller vortex diameter of 139 km and relatively fast translation speed of $U_h \sim 6$ ms^{-1} (equation (1)). Additional simulation also shows that if increasing Chan-Hom's transit time to 20 h (red dotted curve in Figure 11a), it would be able to reach the same -2.5°C cooling (green bullet in Figure 10a) as Lupit did. In addition, Chan-Hom's wind speed was weaker than Lupit's. If forcing Chan-Hom's profile (Figure 11b) using Lupit's 145 kts wind, it would

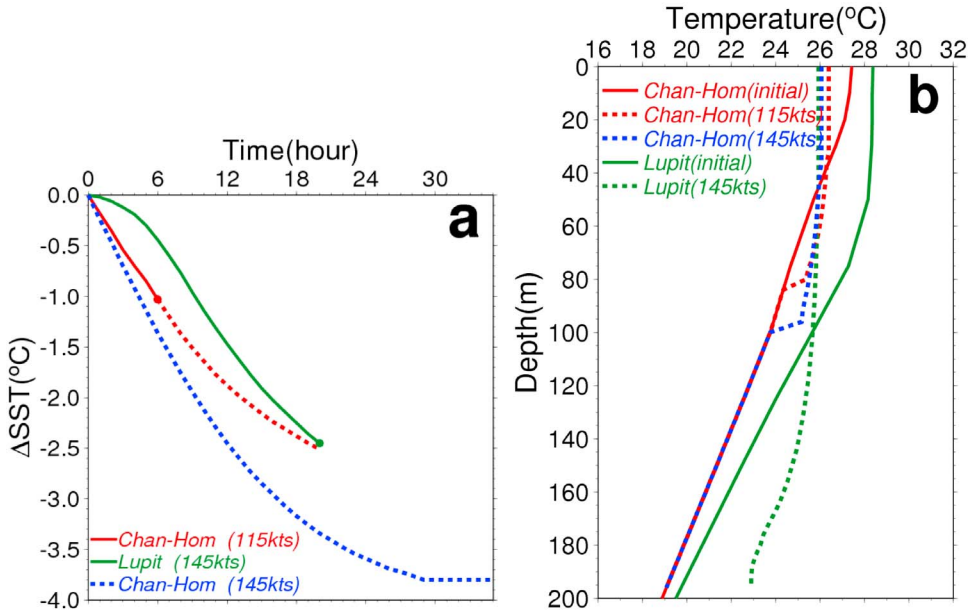

Figure 11. (a) Comparison of SST cooling response for Chan-Hom case (115 kts), Lupit case (145 kts), and Chan-Hom case but forced by the 145 kts wind of Lupit. Color bullets denote the SST cooling at the end of the transit time. (b) Comparison of the pretyphoon (solid profiles) and after-typhoon (at the end of transit time, dashed profiles) depth-temperature profiles for the two cases.

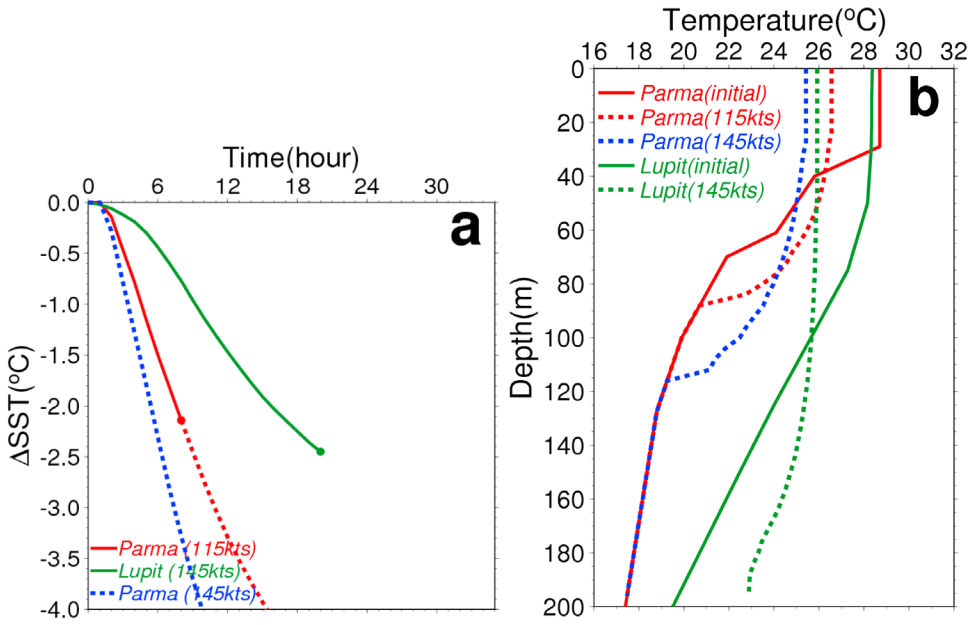

Figure 12. (a and b) As in Figure 11 but for the comparison between Parma and Lupit cases.

take even less time, i.e., 9 h to reach Lupit's cooling response (blue dotted curve in Figure 11a).

[22] As for Parma case, the situation was very similar to Chan-Hom's. In Figure 12a, one can see that due to its shorter transit time, Parma's response (red bullet) was weaker than Lupit's (green bullet). It can also be noted that if given the same wind speed of 145 kts, it takes much shorter time for Parma (4 h) than Lupit (20 h) to reach the same cooling response of ∼−2.5°C (blue dotted curve in Figure 12a). This is due to difference in the ocean precondition that Parma passed by a region with cold water closer to the surface than in the Lupit case (Figure 12b). From Figure 12b, it can be observed that the mixed layer for the Parma case was ∼30 m with D26 ∼ 40 m while in the Lupit case, the mixed layer was ∼60 m and D26 ∼ 90 m. In other words, the preexisting ocean condition of Parma was more favorable to induce stronger ocean response because the cold water was closer to the surface. However, due to Parma's insufficient wind speed and transit time, it was not able to induce same amount of cooling as Lupit did (Figure 12a).

4.4. Category 2 Cases: Etau (Peak Intensity: 95 kts) and Dujuan (Peak Intensity: 95 kts)

[23] Examining the situation for category 2 typhoon Etau, the weaker ocean's response was also due to weak wind and short transit time. It could be found that if using the observed

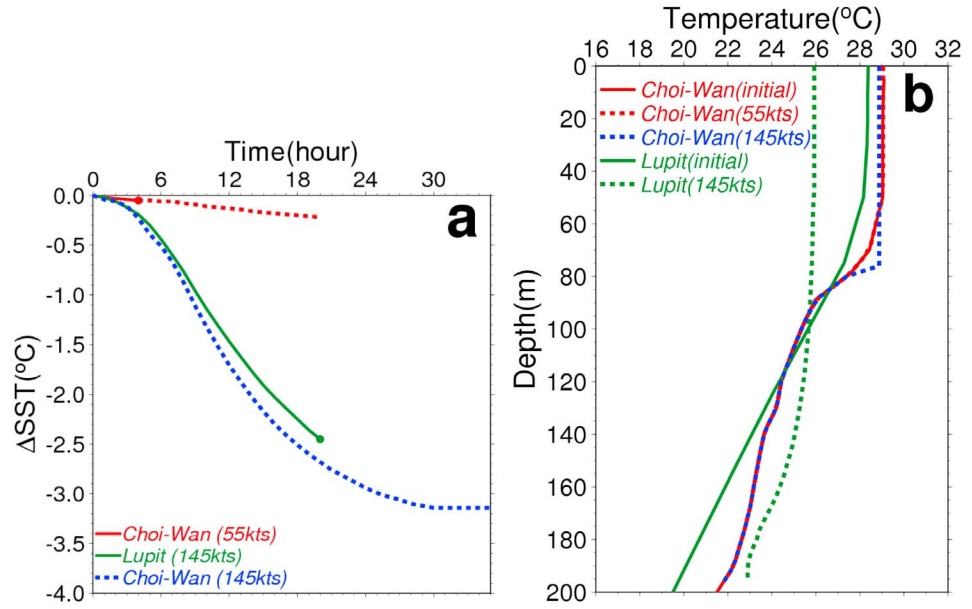

Figure 13. As in Figure 11 but for the comparison between Choi-Wan and Lupit cases.

Table 2. Weekly Primary Production Estimation Based on the VGPM Model for the Ketsana-Induced Bloom Event[a]

VGPM Ketsana	Chl-a Mean[b] (mg m^{-3})	SST Mean[b] (°C)	Bloom Area (m^2)	IPP Mean[b] (mg C m^{-2} D^{-1})	Total Daily Production (mg C D^{-1})	Total Weekly Production (mg C)	SST Threshold (°C)
2003 1026-1101	0.13 (0.07)	25.77 (0.64)	3.85e+11	333.16 (120.44)	1.29e+14	9.00e+14	26.5
2003 1102-1108	0.07 (0.02)	26.52 (0.32)	3.34e+11	188.52 (39.94)	6.30e+13	4.41e+14	27.0

[a]The weekly averaged Chl-a (in mg m^{-3}), weekly averaged SST (°C), bloom patch area (in m^2), weekly averaged integrated primary productivity (IPP) (in mg C m^{-2} D^{-1}), total daily primary production (by integrating IPP over the bloom patch area), and total weekly production (by integrating daily primary production by 7 days) for each of the two weeks are summarized. Total production (mg C): 1.34e+15. As SeaWiFS Chl-a observation can be obscured by cloud and causes underestimation of the bloom area, the bloom area is estimated based on the area of SST cooling using the SST threshold.

[b]Standard deviation is given in parentheses.

category 2, 95 kts wind of Etau and given Etau's transit time of only 5 h, the cooling response was very weak, ~−0.7°C. However, if prolonging the transit time to 20 h as Lupit's transit time, even stronger cooling than Lupit could be induced. If without increase in transit time, another way to induce strong cooling is through increase in wind speed. If increasing Etau's wind speed to Lupit's 145 kt, it would only take 4 h to reach the same response as Lupit's. The simulation results for Dujuan case was found to be similar to Etau. Again due to weak wind (category 2) and short transit time of 7 h, the ocean's response was weak with SST cooling of ~−1.2°C. Through increase in wind speed or transit time, it became possible to reach similar amount of cooling response as Lupit did.

4.5. Category 1 Case: Krovanh (Peak Intensity: 65 kts)

[24] As Krovanh was an even weaker typhoon of only category 1, the ocean's response was very small. Given its transit time of 5 h, the ocean's response in SST cooling was only ~0.1°C. Clearly the wind was too weak and transit time was too short to induce any significant response. If wind speed and transit time could be increased, stronger response could be induced.

4.6. Tropical Storm Cases: Koppu (Peak Intensity: 60 kts), Choi-Wan (Peak Intensity: 55 kts), and Yan-Yan (Peak Intensity: 40 kts)

[25] As for the 3 tropical storm cases (i.e., Koppu, Choi-Wan, and Yan-Yan), since they were the weakest and their transit time was also short (3–7 h, Table 1), the responses were very minimal (Figure 13). The cooling response for Koppu at the corresponding transit time (7 h) was −0.4°C, for Choi-Wan was −0.1°C (transit time 4 h, see Figure 13), and ~0°C (transit time 3 h) for Yan-Yan. It was noted that though the initial D26 for the Yan-Yan case was the deepest among all cases (Table 1). Thus together with the very weak wind of Yan-Yan, the cooling response was ~0°C.

4.7. Discussion

[26] From the series of numerical experiments, it can be seen that it is necessary to consider four factors. The first is typhoon's intensity, as it is the wind forcing to induce ocean's response. The second and third are typhoon's translation speed and size in vortex diameter, because they determine the transit time. The forth factor is ocean's precondition, since it determines how deep (or how shallow) the cold, nutrient-rich water lies. Any one of the above factor being unfavorable would lead to weakening in response. Especially in the WNPSO the mixed layer and nutricline are deep [*Garcia et al.*, 2006]. In other words, even with intense wind but if the transit time is short or the precondition was unfavorable, the ocean's response can still be weak. On the other hand, even with favorable precondition and long transit time but without sufficiently strong wind, it will still not be possible to induce strong ocean response.

[27] The reasons for the weak responses of the nine cases besides Lupit and Ketsana are summarized. For the case of Maemi, it was due to unfavorable ocean precondition because it encountered two prominent warm ocean eddies which acted as insulators to restrain the cold, nutrient-rich water to be entrained to the surface layer. Due to insufficient wind speed and short transit time (caused by small storm size and/or fast translation speed), the responses of Chan-Hom, Parma, Dujuan, Etau, Krovanh, Koppu, Choi-Wan, and Yan-Yan were weak. As a result, only two (Lupit and Ketsana) out of eleven typhoons passing over the WNPSO in 2003 could induce sufficient biological and SST cooling responses.

5. Impact on Primary Production

[28] Using the VGPM model [*Behrenfeld and Falkowski*, 1997] with input from satellite-observed Chl-a and SST, the primary productivity increase induced by Ketsana and Lupit was calculated (Tables 2 and 3). As illustrated in Figure 14a, the increase in integrated primary production (IPP) from the Ketsana event reached 300–800 mg C m^{-2} D^{-1} while the climatological IPP of October in the WNPSO is typically around 140–160 mg C m^{-2} D^{-1} (Figure 14b). The bloom was found to last for 2 weeks (Figure 15) and the total primary production in carbon fixation was estimated to be 1.34×10^{15} mg C (Table 2). Similarly, due to the impact of supertyphoon Lupit, the IPP increased to 300–600 mg C

Table 3. As in Table 2 but for the Lupit Event[a]

VGPM Lupit	Chl-a Mean[b] (mg m^{-3})	SST Mean (°C)	Bloom Area (m^2)	IPP Mean (mg C m^{-2} D^{-1})	Total Daily Production (mg C D^{-1})	Total Weekly Production (mg C)	SST (°C) Threshold
2003 1201-1207	0.14 (0.05)	24.71 (0.57)	3.96e+11	327.62 (85.19)	1.30e+14	9.08e+14	25.5
2003 1208-1214	0.13 (0.06)	24.72 (0.68)	4.59e+11	318.67 (91.04)	1.46e+14	1.02e+15	25.6

[a]Total production (mg C): 1.93e+15. As SeaWiFS Chl-a observation can be obscured by cloud and causes underestimation of the bloom area, the bloom area is estimated based on the area of SST cooling using the SST threshold.

[b]Standard deviation is given in parenthesis.

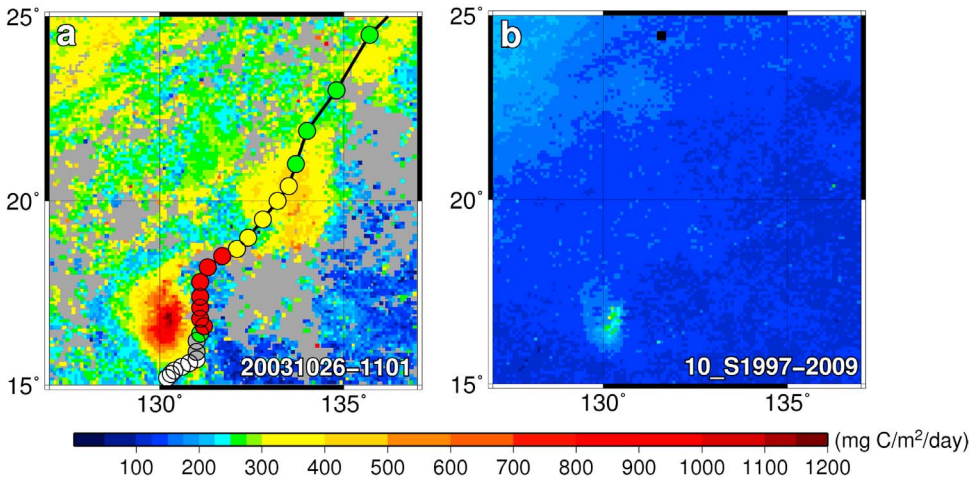

Figure 14. (a) Increase in integrated primary productivity found after Ketsana's passing as compared to (b) climatology.

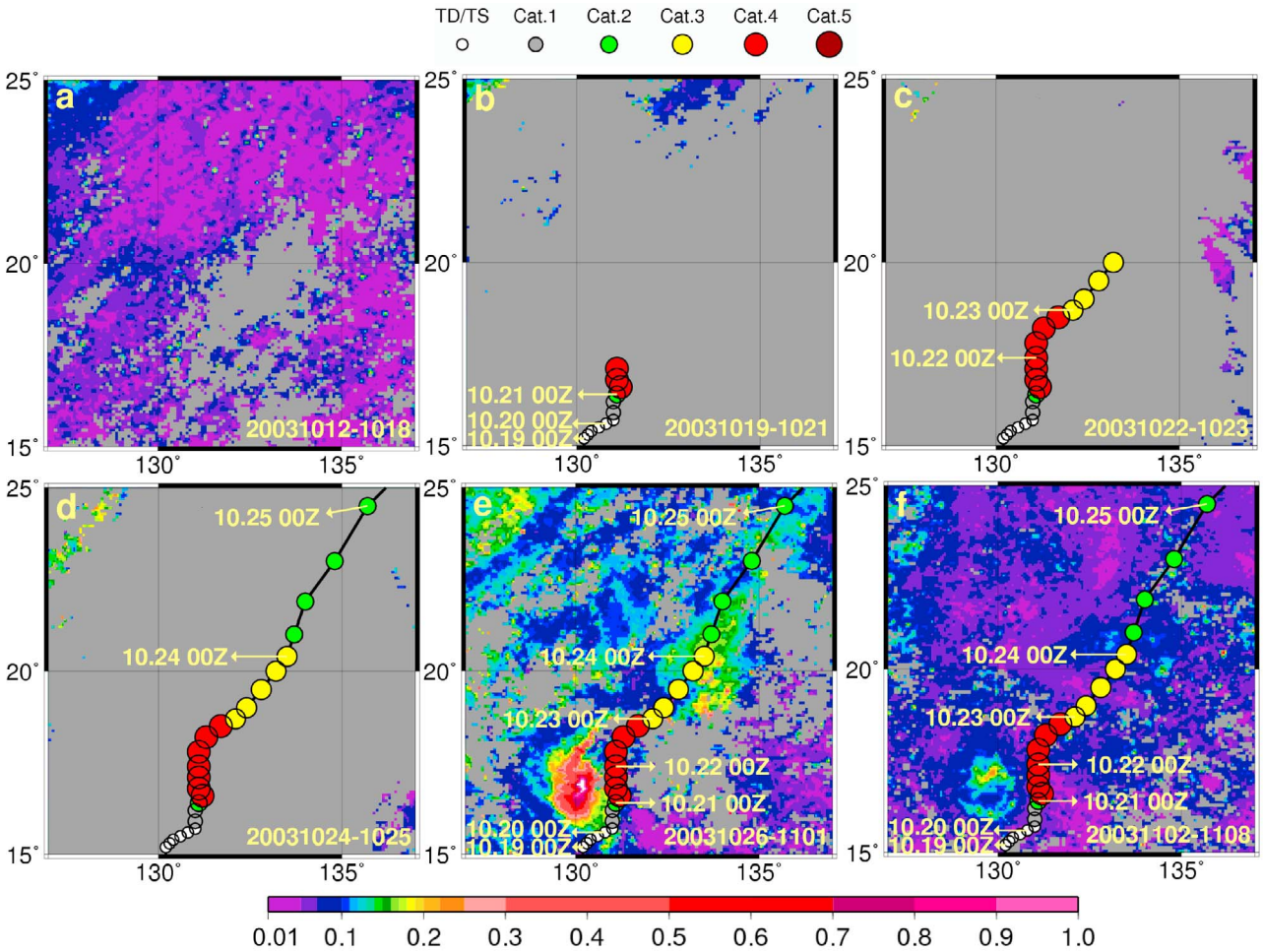

Figure 15. Sequence of pretyphoon and posttyphoon SeaWiFS Chl-a observation for the Ketsana case. The track of Ketsana is overlaid.

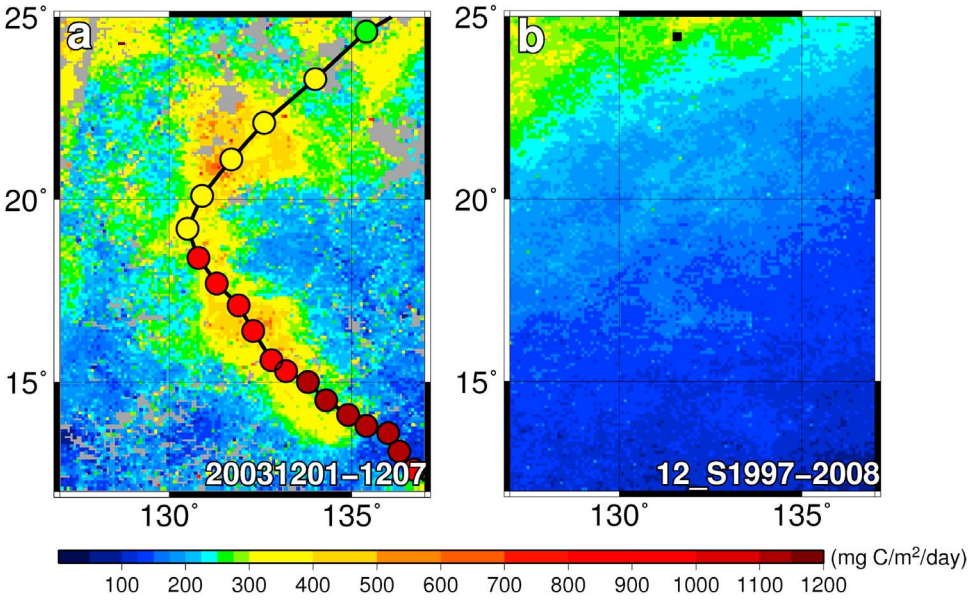

Figure 16. (a and b) As in Figure 14 but for Lupit case.

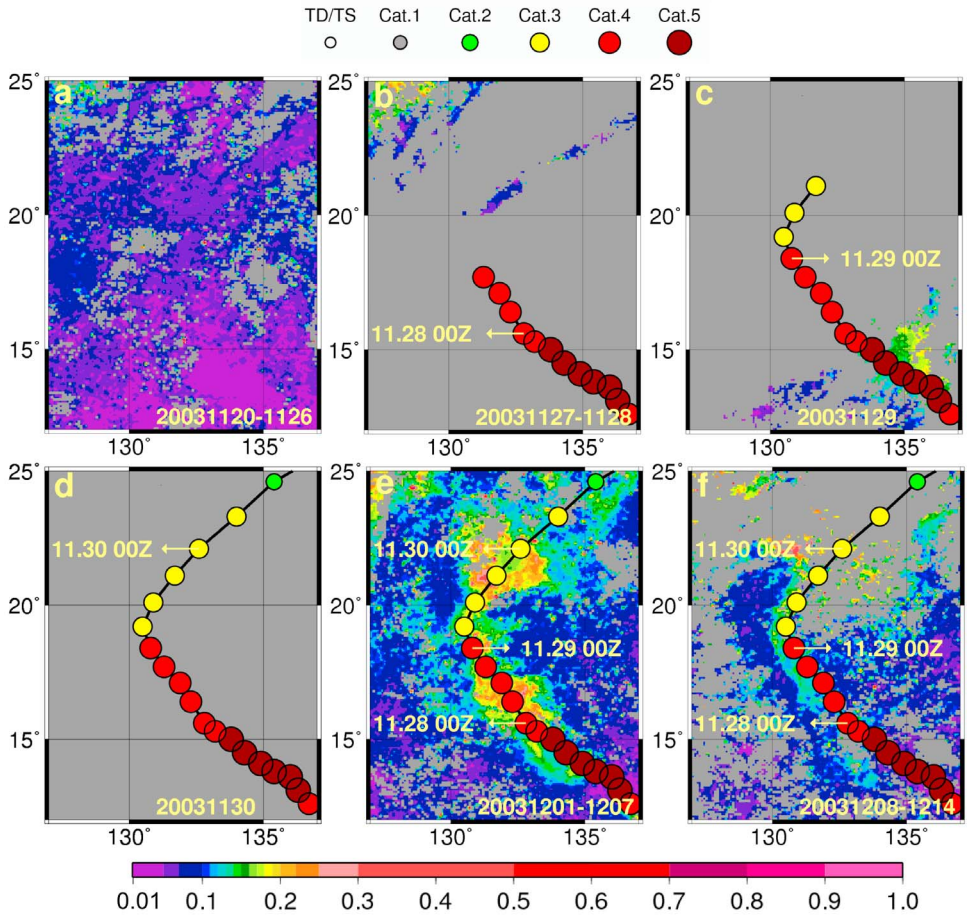

Figure 17. As in Figure 15 but for Lupit case.

m^{-2} D^{-1} (Figure 16a), as compared to the climatological IPP in December of ~140–200 mg C m^{-2} D^{-1} (Figure 16b). This event also lasted for two weeks (Figure 17) and the estimated carbon fixation was 1.93×10^{15} mg C (Table 3).

[29] From above, the total annual primary production increase by typhoons in the WNPSO was estimated to be 3.27×10^{15} mg C (0.00327 Pg), equivalent to 0.15% of the global ocean annual anthropogenic CO_2 uptake of 2.2 Pg and 0.0073% of the global ocean annual primary production of 45 Pg [*Falkowski et al.*, 1998; *Manning and Keeling*, 2006; *Canadell et al.*, 2007]. This suggests that though WNPSO has the highest number and intensity of tropical cyclones among the world oceans, tropical cyclones in the WNPSO have little contribution to enhance biological carbon fixation in the context of global carbon-climate system. Furthermore, as typhoon-induced responses involves deeper-ocean nutrient pumping, deeper ocean CO_2 could also be brought to the upper ocean to offset the biological carbon drawdown [*Bates et al.*, 1998]. As a result, the net impact could be even smaller.

6. Conclusions

[30] Using multiple remote sensing observations and series of numerical experiments, this work systematically investigates typhoon-induced phytoplankton blooms in the western North Pacific subtropical ocean for 1 year in 2003. It was found the following.

[31] 1. Among the eleven typhoon cases, only two typhoons (Ketsana and Lupit) were able to induce phytoplankton blooms in the WNPSO. In the case of Ketsana, the observed Chl-a concentration increased from the pretyphoon value of ≦0.1 mgm^{-3} to 0.3–0.8 mgm^{-3} and the associated SST cooling was ~−2.5 to −6.5°C. For the case of Lupit, Chl-a concentration increased to ~0.3–0.4 mgm^{-3} and the associated SST cooling was ~−2.5 to −3.5°C.

[32] 2. The reason for such low percentage (2/11 = 18%) was that in addition to wind speed, it was also necessary to consider typhoon's translation speed, size (vortex diameter), and precondition because translation speed and size affect transit time while precondition determines where cold, nutrient-rich water lies. Failing to meet any one of the conditions above could weaken ocean's responses in the WNPSO because the mixed layer and nutricline are deep. As such, besides from Lupit and Ketsana, none of the other typhoons were able to induce sufficient responses.

[33] 3. Due to encountering of two preexisting prominent warm ocean eddies, even the most intense supertyphoon on Earth in 2003, i.e., Maemi, was not able to induce phytoplankton blooms in the WNPSO. The robust warm eddies effectively deepened the mixed layer and kept the cold, nutrient rich water at depth. It acted as an effective insulator to restrain ocean's response. Even at the 150 kts category 5 wind, ocean's SST cooling was restrained to be ≦−1.5°C and little biological response could be observed. As such, the observed two blooms were caused by the second (Lupit) and the third (Ketsana) intense typhoons passing the WNPSO, but not the most intense typhoon Maemi.

[34] 4. Due to insufficient wind speed and transit time (because of fast translation speed and small size), all the other eight typhoons, Chan-Hom (category 4), Parma (category 4), Dujuan (category 2), Etau (category 2), Krovanh (category 1), Koppu (tropical storm), Choi-Wan (tropical storm), and Yan-Yan (tropical storm), were not able to induce phytoplankton blooms. The corresponding SST cooling was also weak, typically between 0 and −1.5°C.

[35] 5. Based on this work, it was observed that for typhoons to induce phytoplankton blooms in the WNPSO, it requires (1) not encountering preexisting prominent warm ocean eddy; (2) intense upper category 4 or 5 wind speed of ≧125–145 kts; and (3) sufficiently long transit time of ≧20–34 h (achieved by slow translation speed of ≦1.7–3.6 ms^{-1} and relatively large typhoon size of ≧210–257 km (based on 64 kts wind diameter)).

[36] 6. The total annual primary production increase by typhoons in the WNPSO was estimated to be ~3.27×10^{15} mg C (0.00327 Pg). This is equivalent to 0.15% of the global annual anthropogenic CO_2 uptake of ~2.2 Pg. Further, as typhoon-induced ocean responses are accompanied by deeper-ocean pumping, deeper ocean CO_2 could also be brought to the surface to further offset the biological CO_2 drawdown. This suggests that though WNPSO is the region where most intense typhoons occur on Earth, WNPSO typhoons have little contribution to enhance biological carbon fixation in the context of global carbon-climate system.

[37] **Acknowledgments.** The author wishes to thank Chun-Chi Lien, Chih-Wei Huang, and Iam-Fei Pun for help in data processing. Thanks also to the U.S. NASA, NOAA, the AVISO altimetry team, the Remote Sensing Systems, and the Argo float team for data provision. This work is supported by the National Science Council, Taiwan, through NSC 98-2611-M-002-014-MY3W and NSC 100-2111-M-002-001 and National Taiwan University project 10R70803.

References

Ali, M. M., P. S. V. Jagadeesh, I.-I. Lin, and J.-Y. Hsu (2012), A neural network approach to estimate tropical cyclone heat potential in the Indian Ocean, *IEEE Geosci. Remote Sens. Lett.*, in press.

Babin, S. M., J. A. Carton, T. D. Dickey, and J. D. Wiggert (2004), Satellite evidence of hurricane-induced phytoplankton blooms in an oceanic desert, *J. Geophys. Res.*, *109*, C03043, doi:10.1029/2003JC001938.

Bates, N. R., A. H. Knap, and A. F. Michaels (1998), Contribution of hurricanes to local and global estimates of air-sea exchange of CO_2, *Nature*, *395*, 58–61, doi:10.1038/25703.

Behrenfeld, M. J., and P. G. Falkowski (1997), Photosynthetic rates derived from satellite-based chlorophyll concentration, *Limnol. Oceanogr.*, *42*(1), 1–20, doi:10.4319/lo.1997.42.1.0001.

Canadell, J. G., C. L. Le Quéré, M. R. Raupach, C. B. Field, E. T. Buitenhuis, P. Ciais, T. J. Conway, N. P. Gillett, R. A. Houghton, and G. Marland (2007), Contributions to accelerating atmospheric CO_2 growth from economic activity, carbon intensity, and efficiency of natural sinks, *Proc. Natl. Acad. Sci. U. S. A.*, *104*, 18,866–18,870, doi:10.1073/pnas.0702737104.

Carder, K. L., F. R. Chen, Z. P. Lee, S. K. Hawes, and D. Kamykowski (1999), Semianalytic Moderate-Resolution Imaging Spectrometer algorithms for chlorophyll-a and absorption with bio-optical domains based on nitrate-depletion temperatures, *J. Geophys. Res.*, *104*, 5403–5421, doi:10.1029/1998JC900082.

Chang, Y., H. T. Liao, M. A. Lee, J. W. Chan, W. J. Shieh, K. T. Lee, G. H. Wang, and Y. C. Lan (2008), Multisatellite observation on upwelling after the passage of Typhoon Hai-Tang in the southern East China Sea, *Geophys. Res. Lett.*, *35*, L03612, doi:10.1029/2007GL032858.

Cione, J. J., and E. W. Uhlhorn (2003), Sea surface temperature variability in hurricanes: Implications with respect to intensity change, *Mon. Weather Rev.*, *131*, 1783–1796, doi:10.1175//2562.1.

D'Asaro, E., et al. (2011), Typhoon-ocean interaction in the western North Pacific, Part 1, *Oceanography*, *24*(4), 24–31, doi:10.5670/oceanog.2011.91.

Dickey, T., D. Frye, J. McNeil, D. Manov, N. Nelson, D. Sigurdson, H. Jannasch, D. Siegel, T. Michaels, and R. Johnson (1998), Upper-ocean temperature response to Hurricane Felix as measured by the Bermuda Testbed Mooring, *Mon. Weather Rev.*, *126*, 1195–1201, doi:10.1175/1520-0493(1998)126<1195:UOTRTH>2.0.CO;2.

Falkowski, P., R. T. Backer, and V. Smetacek (1998), Biogeochemical controls and feedbacks on ocean primary production, *Science*, *281*, 200–206, doi:10.1126/science.281.5374.200.

Falkowski, P., et al. (2000), The global carbon cycle: A test of our knowledge of Earth as a system, *Science*, *290*, 291–296, doi:10.1126/science.290.5490.291.

Fu, L. L., and A. Cazenave (Eds.) (2001), *Satellite Altimetry and Earth Sciences: A Handbook of Techniques and Applications*, 463 pp., Academic, San Diego, Calif.

Fu, L. L., E. J. Christensen, C. A. Yamarone, M. Lefebvre, Y. Menard, M. Dorrer, and P. Escudier (1994), TOPEX/POSEIDON mission overview, *J. Geophys. Res.*, *99*, 24,369–24,381, doi:10.1029/94JC01761.

Garcia, H. E., R. A. Locarnini, T. P. Boyer, and J. I. Antonov (2006), *World Ocean Atlas 2005, vol. 4, Nutrients (Phosphate, Nitrate, and Silicate)*, *NOAA Atlas NESDIS*, vol. 64, edited by S. Levitus, 396 pp., NOAA, Silver Spring, Md.

Goni, G., et al. (2009), Application of satellite-derived ocean measurements to tropical cyclone intensity forecasting, *Oceanography*, *22*(3), 190–197, doi:10.5670/oceanog.2009.78.

Gould, J., et al. (2004), Argo profiling floats bring new era of in situ ocean observations, *Eos Trans. AGU*, *85*(19), 185.

Jacob, S. D., L. K. Shay, A. J. Mariano, and P. G. Black (2000), The 3D oceanic mixed layer response to hurricane Gilbert, *J. Phys. Oceanogr.*, *30*, 1407–1429, doi:10.1175/1520-0485(2000)030<1407:TOMLRT>2.0.CO;2.

Keeley, B., C. Sun, and L. P. Villeon (2003), Global temperature and salinity profile program annual report, report, 32 pp., NOAA, Silver Spring, Md.

Kim, H. M., C. D. Hoyos, P. J. Webster, and I. S. Kang (2010), Ocean-atmosphere coupling and the boreal winter MJO, *Clim. Dyn.*, *35*(5), 771–784, doi:10.1007/s00382-009-0612-x.

Kug, J. S., F. F. Jin, and S. I. An (2009), Two types of El Niño events: Cold tongue El Niño and warm pool El Niño, *J. Clim.*, *22*, 1499–1515, doi:10.1175/2008JCLI2624.1.

Lin, I.-I., W. T. Liu, C.-C. Wu, J. C. H. Chiang, and C.-H. Sui (2003a), Satellite observations of modulation of surface winds by typhoon-induced upper ocean cooling, *Geophys. Res. Lett.*, *30*(3), 1131, doi:10.1029/2002GL015674.

Lin, I., W. T. Liu, C.-C. Wu, G. T. F. Wong, C. Hu, Z. Chen, W.-D. Liang, Y. Yang, and K.-K. Liu (2003b), New evidence for enhanced ocean primary production triggered by tropical cyclone, *Geophys. Res. Lett.*, *30*(13), 1718, doi:10.1029/2003GL017141.

Lin, I.-I., C.-C. Wu, K. A. Emanuel, I.-H. Lee, C.-R. Wu, and I.-F. Pun (2005), The Interaction of Supertyphoon Maemi (2003) with a warm ocean eddy, *Mon. Weather Rev.*, *133*, 2635–2649, doi:10.1175/MWR3005.1.

Lin, I.-I., C.-C. Wu, I.-F. Pun, and D.-S. Ko (2008), Upper-ocean thermal structure and the western North Pacific category-5 typhoons. Part I: Ocean features and category-5 typhoon's intensification, *Mon. Weather Rev.*, *136*, 3288–3306, doi:10.1175/2008MWR2277.1.

Lin, I.-I., I.-F. Pun, and C.-C. Wu (2009a), Upper-ocean thermal structure and the western North Pacific category-5 typhoons. Part II: Dependence on translation speed, *Mon. Weather Rev.*, *137*, 3744–3757, doi:10.1175/2009MWR2713.1.

Lin, I.-I., C.-H. Chen, I.-F. Pun, W. T. Liu, and C.-C. Wu (2009b), Warm ocean anomaly, air sea fluxes, and the rapid intensification of tropical cyclone Nargis (2008), *Geophys. Res. Lett.*, *36*, L03817, doi:10.1029/2008GL035815.

Lin, I.-I., C.-C. Lien, C.-R. Wu, G. T. F. Wong, C.-W. Huang, and T.-L. Chiang (2010), Enhanced primary production in the oligotrophic South China Sea by eddy injection in spring, *Geophys. Res. Lett.*, *37*, L16602, doi:10.1029/2010GL043872.

Lin, I.-I., et al. (2011a), Fertilization potential of volcanic dust in the low-nutrient low-chlorophyll western North Pacific subtropical gyre: Satellite evidence and laboratory study, *Global Biogeochem. Cycles*, *25*, GB1006, doi:10.1029/2009GB003758.

Lin, I.-I., M.-D. Chou, and C.-C. Wu (2011b), Warm ocean eddy's impact on typhoon Morakot (2009): A prelimenary study from remote sensing and numerical modelling, *Terr. Atmos. Oceanic Sci.*, *22*(6), 661–671, doi:10.3319/TAO.2011.08.19.01(TM).

Liu, W. T., W. Tang, and P. S. Polito (1998), NASA scatterometer provides global ocean-surface wind fields with more structures than numerical weather prediction, *Geophys. Res. Lett.*, *25*, 761–764, doi:10.1029/98GL00544.

Manning, A. C., and R. F. Keeling (2006), Global oceanic and land biotic carbon sinks from the Scripps atmospheric oxygen flask sampling network, *Tellus, Ser. B*, *58*(2), 95–116, doi:10.1111/j.1600-0889.2006.00175.x.

McPhaden, M. J. (1999), Genesis and evolution of the 1997–98 El Niño, *Science*, *283*, 950–954, doi:10.1126/science.283.5404.950.

Mellor, G. L., and T. Yamada (1982), Development of a turbulence closure model for geophysical fluid problems, *Rev. Geophys.*, *20*, 851–875, doi:10.1029/RG020i004p00851.

O'Reilly, J. E., S. Maritorena, B. G. Mitchell, D. A. Siegel, K. L. Carder, S. A. Garver, M. Kahru, and C. R. McClain (1998), Ocean color chlorophyll algorithms for SeaWiFS, *J. Geophys. Res.*, *103*, 24,937–24,953, doi:10.1029/98JC02160.

Powell, M. D., P. J. Vickery, and T. A. Reinhold (2003), Reduced drag coefficient for high wind speeds in tropical cyclones, *Nature*, *422*, 279–283, doi:10.1038/nature01481.

Price, J. F. (1981), Upper ocean response to a hurricane, *J. Phys. Oceanogr.*, *11*, 153–175, doi:10.1175/1520-0485(1981)011<0153:UORTAH>2.0.CO;2.

Price, J. F., T. B. Sanford, and G. Z. Forristall (1994), Forced stage response to a moving hurricane, *J. Phys. Oceanogr.*, *24*, 233–260, doi:10.1175/1520-0485(1994)024<0233:FSRTAM>2.0.CO;2.

Pun, I. F., I.-I. Lin, C. R. Wu, D. S. Ko, and W. T. Liu (2007), Validation and application of altimetry-derived upper ocean thermal structure in the western north pacific ocean for typhoon intensity forecast, *IEEE Trans. Geosci. Remote Sens.*, *45*, 1616–1630, doi:10.1109/TGRS.2007.895950.

Pun, I. F., Y.-T. Chang, I.-I. Lin, T.-Y. Tang, and R.-C. Lien (2011), Typhoon-ocean interaction in the western north Pacific, Part 2, *Oceanography*, *24*(4), 32–41, doi:10.5670/oceanog.2011.92.

Sabine, C. L., et al. (2004), The oceanic sink for anthropogenic CO_2, *Science*, *305*, 367–371, doi:10.1126/science.1097403.

Sanford, T. B., J. F. Price, and J. B. Girton (2011), Upper ocean response to Hurricane Frances (2004) observed by profiling EM-APEX floats, *J. Phys. Oceanogr.*, *41*, 1041–1056, doi:10.1175/2010JPO4313.1.

Shang, S. L., L. Li, F. Sun, J. Wu, C. Hu, D. Chen, X. Ning, Y. Qiu, C. Zhang, and S. Shang (2008), Changes of temperature and bio-optical properties in the South China Sea in response to typhoon Lingling, 2001, *Geophys. Res. Lett.*, *35*, L10602, doi:10.1029/2008GL033502.

Shay, L. K., G. J. Goni, and P. G. Black (2000), Effects of a warm oceanic feature on Hurricane Opal, *Mon. Weather Rev.*, *128*, 1366–1383, doi:10.1175/1520-0493(2000)128<1366:EOAWOF>2.0.CO;2.

Stephens, C., J. I. Antonov, T. P. Boyer, M. E. Conkright, R. A. Locarnini, T. D. O'Brien, and H. E. Garcia (2002), *World Ocean Atlas 2001, vol. 1, Temperature*, edited by S. Levitus, *NOAA Atlas NESDIS*, vol. 49, NOAA, Silver Spring, Md.

Wentz, F. J., C. Gentemann, D. Smith, and D. Chelton (2000), Satellite measurements of sea surface temperature through clouds, *Science*, *288*, 847–850, doi:10.1126/science.288.5467.847.

Zheng, G., and D. Tang (2007), Offshore and nearshore chlorophyll increases induced by typhoon winds and subsequent terrestrial rainwater runoff, *Mar. Ecol. Prog. Ser.*, *333*, 61–74, doi:10.3354/meps333061.

I.-I. Lin, Department of Atmospheric Sciences, National Taiwan University, Number 1, Section 4, Roosevelt Rd., Taipei 106, Taiwan. (iilin@as.ntu.edu.tw)